



Affordable medium-finesse optical cavity for diode laser stabilization

David Rodríguez Fernández¹ · Manuel Alejandro Lefrán Torres¹ · Marcos Roberto Cardoso¹ ·
Jorge Douglas Massayuki Kondo² · Mark Saffman³ · Luis Gustavo Marcassa¹

Received: 27 November 2023 / Accepted: 28 January 2024 / Published online: 25 March 2024
© The Author(s), under exclusive licence to Springer-Verlag GmbH Germany, part of Springer Nature 2024

Abstract

We have constructed and characterized an affordable medium-finesse optical cavity ($\mathcal{F} \sim 1500$) for the stabilization of tunable diode lasers at two different wavelengths (780, and 960 nm, respectively). Its main element is an ultra-low expansion glass spacer, whose temperature was stabilized using thermoelectric cooler elements inside a vacuum chamber. By combining the dual sideband technique and the classical Pound–Drever–Hall technique, we were able to lock the lasers at any frequency within the cavity free spectral range. The cavity presents a long-term drift of resonant frequency of 1.2 MHz/day, which can be compensated for by temperature variation. Finally, we demonstrate the cavity use in an electromagnetically induced transparency microwave spectrum experiment in a thermal atomic sample.

1 Introduction

Frequency-stabilized lasers have a broad range of applications in basic research and technology. Well known examples are the detection of gravitational waves [1] and high precision clocks for metrology and relativity theory tests [2, 3]. Frequency-stabilized lasers are also extensively employed across various research fields, such as quantum gases, molecular physics, and Rydberg atoms. In the 1940s, Pound pointed out that atomic and molecular transitions in the microwave region could be studied with great precision using a highly stable signal generator [4]. In the 1960s, He–Ne laser [5] frequency stabilization was proposed using as a reference the “burned holes” in the Gaussian emission

profile due to saturation of the amplifier medium, a phenomenon known as Lamb dip [6]. Later, Paul and Michael set the foundation for the development of the now widely used saturation absorption spectroscopy (SAS) [7]. Later, it was improved by polarization spectroscopy [8] and modulation transfer spectroscopy [9]. Such techniques are widely used nowadays because of their simplicity and robustness. However, they have two major disadvantages: (1) the linewidth of the locked laser is determined by the width of the atomic/molecular transition; and (2) the locked frequency is determined by the same transitions, requiring the use of acousto-optic modulators (AOM’s) to lock the laser frequency in a small frequency range near such transitions.

This problem can be solved using the resonance frequency of optical cavities. The position, width, and separation of resonant frequencies are, in theory, tunable with the choice of cavity geometry and reflectivity of its mirrors (finesse). Traditionally, this can be achieved by applying homodyne

David Rodríguez Fernández, Manuel Alejandro Lefrán Torres, Marcos Roberto Cardoso, Jorge Douglas Massayuki Kondo, Mark Saffman and Luis Gustavo Marcassa contributed equally to this work.

✉ David Rodríguez Fernández
davidrf@ifsc.usp.br

Manuel Alejandro Lefrán Torres
lefran@ifsc.usp.br

Marcos Roberto Cardoso
cardosomr@ifsc.usp.br

Jorge Douglas Massayuki Kondo
massayuki.kondo@ufsc.br

Mark Saffman
msaffman@wisc.edu

Luis Gustavo Marcassa
marcassa@ifsc.usp.br

¹ Instituto de Física de São Carlos, Universidade de São Paulo, Avenida Trabalhador São-Carlense, São Carlos, São Paulo 13566-590, Brazil

² Departamento de Física, Universidade Federal de Santa Catarina, Rua Roberto Sampaio Gonzaga, Florianópolis, Santa Catarina 88040-900, Brazil

³ Department of Physics, University of Wisconsin-Madison, University Avenue, Madison, WI 53706-1390, USA

detection to a phase-modulated beam reflected by an optical cavity, with the error signal being electrically fed back into a laser [10]. This is known as the Pound–Drever–Hall (PDH) technique, and it connects the instability of the resonator length to variations of the laser frequency. So, it requires that the optical cavity be isolated from temperature/pressure variations and mechanical vibrations. In general, such cavities are built using ultra-low expansion (ULE) glass and nowadays are commercially available. They serve as workhorses for laser stabilization in atomic physics. However, the majority of experiments do not require a linewidth below 10 kHz. Consequently, it is feasible to fabricate homemade cavities tailored to experiments with lower stability requirements at a reduced cost.

In this work, we have designed, constructed and characterized an affordable medium-finesse optical cavity operating at wavelengths of 780 nm and 960 nm, which is employed for laser stabilization in Rydberg atom experiments. Our setup is based on the design developed by de Hond et al. [11]; however, we have made improvements by utilizing a lighter ULE spacer and achieving temperature stabilization through the use of thermoelectric cooler elements within a vacuum chamber. The cavity presents a long-term drift of the resonant frequency of 1.2 MHz/day, which can be compensated for by temperature variation. To finalize, the cavity use is demonstrated in an electromagnetically induced transparency (EIT) microwave spectrum experiment [12, 13]. Here, we provide a simple recipe for constructing and characterizing an optical cavity, which may be used for hot and cold Rydberg atom experiments as well as other atomic physics experiments.

2 Optical cavity design

We chose to build a 100 mm long plano-concave Fabry–Perot interferometer because: (1) its alignment is simpler than other cavity configurations and (2) its free spectral range and medium finesse will allow us to lock and narrow the frequency of our diode lasers using movable sidebands, as pointed out by de Hond et al. [11]. The cavity is formed by a hollow ULE glass cylinder [14], which is 100 mm long with 25.4 mm external diameter and 21.7 mm internal diameter, respectively (Fig. 1). A hole of 12.7 mm diameter on the side is used for vacuum pumping. The weight of our spacer is ≈ 30 g, which is one order of magnitude lighter than that used by de Hond et al. [11]. At the ends of the spacer, custom-made fused silica mirrors, produced by LAYERTEC, are glued onto it using EPO-TEK 353ND epoxy [15]. The mirrors are spherical with 25 mm diameter and 7 mm thickness. Their radii of curvature are $R_1 = 500$ mm and $R_2 = \infty$, respectively. The reflecting surfaces have a reflectivity of $99.8 \pm 0.1\%$ for 780 and 960 nm, while the back surfaces have an antireflector coating

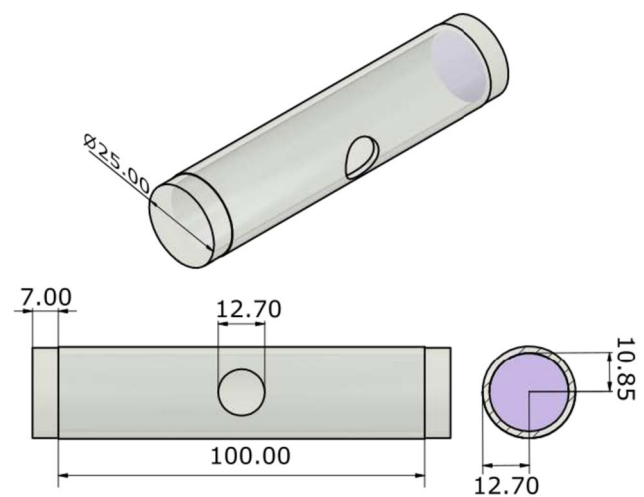


Fig. 1 Drawings of the optical cavity design, which is formed by a 100 mm long ULE spacer with two highly reflective mirrors glued to its ends. The main dimensions are shown

(reflectivity below 0.25%). Figure 1 shows schematic drawings of the optical cavity. This cavity design should present a free spectral range of ($\Delta\nu_{FSR} = c/2L$) 1500 MHz and a finesse of 1500.

3 Temperature stabilization

Small temperature changes (ΔT) will affect the length of the cavity (ΔL), shifting the optical resonance positions by $\Delta\nu$, which is given by [11]:

$$\Delta\nu = \frac{c\alpha\Delta T}{\lambda}, \quad (1)$$

where c is the light speed, λ the laser wavelength, and α the ULE thermal expansion coefficient (upper limit of $30.0 \times 10^{-9} \text{ K}^{-1}$ [14]). If we consider the α upper limit, a laboratory temperature change of $\Delta T = 1$ K over 24 h, $\Delta\nu$ is greater than 10 MHz for $\lambda = 780$ nm, making the cavity unsuitable for laser frequency locking. Therefore, the temperature must be actively stabilized. To implement it, the cavity is housed in a hollow aluminum support cylinder, 135.13 mm long, with an inner diameter 27.4 mm and an outer diameter 51.4 mm, respectively. The cylinder was milled along its axis to form a flat surface with dimensions of $(135.13 \times 35.71 \text{ mm}^2)$. Two Viton rings perfectly fill the gap between the cavity and the cylinder, and they are the only thermal contact between the cavity and the aluminum housing, limiting the temperature stabilization speed. A second aluminum cylinder of 155 mm length and 360.32 mm diameter was also milled along its axis to form a rectangular surface of $(155.00 \times 40.04 \text{ mm}^2)$, which serves as the base of the cavity housing (Fig. 2a). Three thermoelectric coolers

(TEC model RC12-8L, Marlow Industries) were installed between these parts, to stabilize the cavity temperature. Vacuum thermal grease (Apiezon M grease) was applied on TEC's and cylinders to increase thermal conductivity. Four negative thermal coefficient thermistors (NTC model 1600-10 K, Arroyo Instruments) were glued with vacuum epoxy (Epoxy Patch 432037) to the outer surface of the support cylinder, as shown in Fig. 2b. The temperature controller

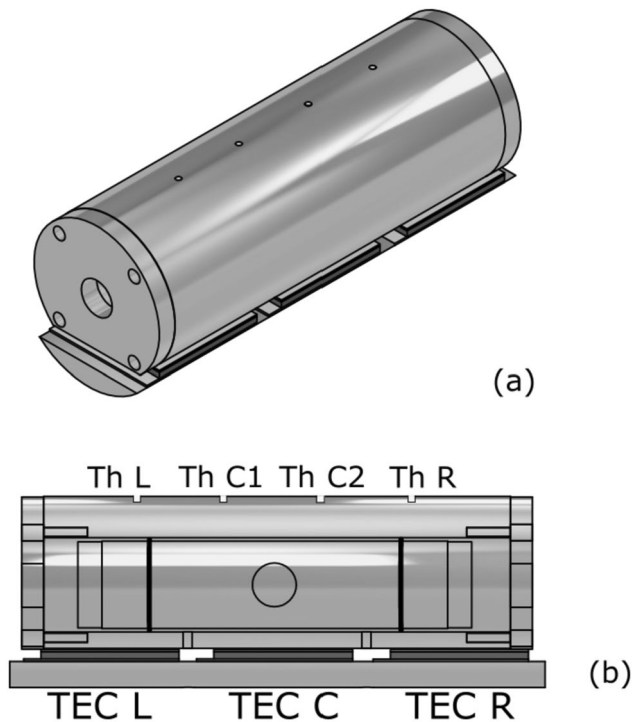


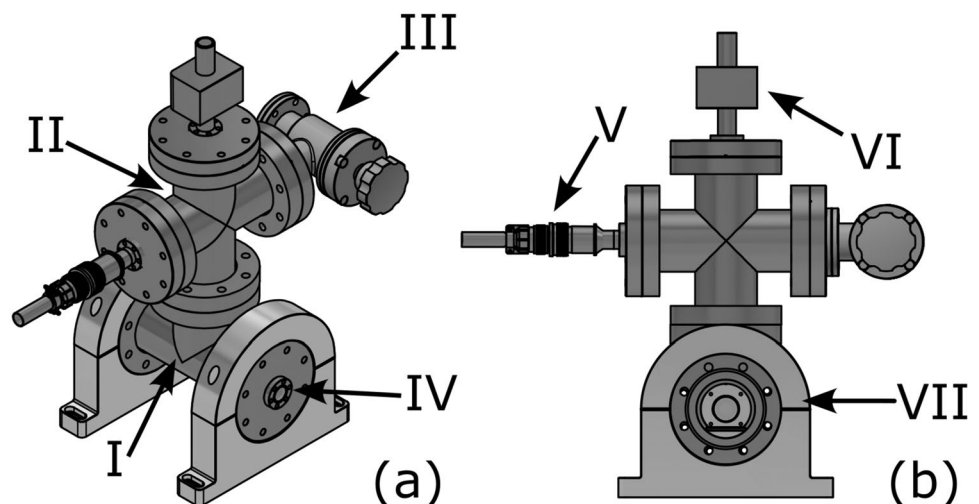
Fig. 2 Schematic drawing of the aluminum support cylinder, which houses the optical cavity. Three thermoelectric coolers (TEC L, TEC C and TEC R) and four thermistors (Th L, Th C1, Th C2 and Th R) were installed to stabilize the temperature

(TECSource 5240, Arroyo Instruments) has a precision of 10 mK and a temperature stability of 4 mK. The center-left thermistor (Th C1) feeds back to the temperature controller, while the other three thermistors monitor the temperature gradient through the system. Finally, two aluminum caps were screwed onto the ends of the cylinder, with a diameter hole 12.70 mm, allowing optical access (Fig. 2a). Detailed drawings are available in the Supplementary Material. The whole system, cavity and aluminum housing, was placed inside a high vacuum setup, which will be discussed in the next section.

4 Vacuum system

To isolate the cavity from air flux and environmental temperature change, the optical cavity and aluminum housing (Fig. 2b) were placed inside a vacuum setup. The vacuum system is made up of several standard stainless steel vacuum parts (from MDC precision): (1) a tee (PN 404038) (I in Fig. 3a); (2) a 4-way cross (PN 405031) (II in Fig. 3a); (3) an all metal angle valve (PN 314006) (III in Fig. 3a); (4) two UV grade fused silica viewports (PN 9722013) (IV in Fig. 3a); (5) a multipin feedthrough (PN 9131002) (V in Fig. 3b); (6) two zero length reducers (PN 150006 and 150008), which have an antireflector coating (reflectivity below 0.5%) in both surfaces. Vacuum thermal grease was also applied between the base cylinder and the tee to improve the thermal conductivity. Kapton insulated copper wires (PN: 113094 and 112088, Accu-Glass Product Inc.) and PTFE teflon shrink tubing (PN: 111316, Accu-Glass Product Inc.) were used for the electrical connections of the TEC's and thermistors. An ion pump (Agilent 2 L/s) (VI in Fig. 3b), was dedicated to keep the vacuum in the system. The entire system was installed on aluminum supports (VII in Fig. 3b) to guarantee mechanical stability.

Fig. 3 Drawings of **a** side view of the system; **b** system with the cavity mounted inside. The principal elements of the vacuum system are pointed out as follows: (I) tee; (II) 4-way cross; (III) all metal angle valve; (IV) two UV grade fused silica viewports; (V) multipin feedthrough, (VI) ion pump, and (VII) aluminum supports



After the system was assembled, it was evacuated using a turbo pump, while heated to a temperature of 50 °C. After one week, the pressure was 4×10^{-7} torr. At this point, the ion pump was turned on, the valve was closed, and the turbo pump was turned off and disconnected. The final pressure is the order of 10^{-8} torr (derived from the ion pump current).

5 Experimental setup and optical sideband generation

Here, we describe the experimental setup used to implement frequency locking of two frequency diode lasers (DL Pro, Toptica), operating at 960 and 780 nm, simultaneously in the same optical cavity using the Dual sideband (DSB) locking technique [16]. The experimental setup is shown in Fig. 4a; about 1 mW of power of each laser is coupled to a lithium niobate electro-optic modulator (EOM) (either PM-0S5-10-PFA-PFA-780 or PM-0S5-10-PFA-PFA-960 for 780 and 960 nm, respectively, EOSpace). The frequency of the movable sidebands was generated using a controllable RF source (SynthUSBII model, WindFreak Technologies, LLC). Such a generator operates from 34 to 4400 MHz, covering the full FSR of the cavity, which can be controlled by either the manufacturer's software or Python codes. However, its power output is insufficient to drive the fiber-based EOMs. To address this, we incorporated a 20 dB low-noise amplifier (model ZFL-1000LN+ by Mini-Circuits), whose output was injected into a lithium niobate EOM. The second modulation frequency, for the Pound–Drever–Hall locking scheme [17], is generated by the Digilock 110 module (Toptica) at fractions of 25 MHz. Both RF signals are combined in a 2-way power splitter (model ZFSC-2-1W+, Minicircuits), whose output was injected into a lithium niobate EOM. The electronic DSB modulation system is shown in Fig. 4b. At the modulator output, the single-mode PM fiber delivers a linear polarized Gaussian beam ($\sim 300 \mu\text{W}$), which is matched to the HG_{00} mode of the cavity using lenses (L) and mirrors (M). In our case, we chose that each wavelength enters the cavity at a different window. Before entering the cavity, the laser beam passes through a PBS and a quarter-wave plate ($\lambda/4$), which will separate the reflection signal, detected by amplified fast photodetectors PD1 and PD2 (model PDA8A2, Thorlabs). This signal is processed by the Digilock 110 module (Toptica) to obtain the PDH error signal, which feeds the PID1 and PID2 Digilock circuits that drive the diode current and piezo voltage, respectively, as shown in Fig. 4b. A dichroic mirror (DM) placed in the back end region of the cavities serves as a mirror for the 780 nm laser to be coupled into the cavity and separates the 960 nm laser transmitted by the cavity. Then, the transmission signal of the 960 nm laser is monitored by a fast photodetector PD3 (model DET10A, Thorlabs) and a laser beam profiler (model LBP-1-USB, Newport). This signal is used to obtain

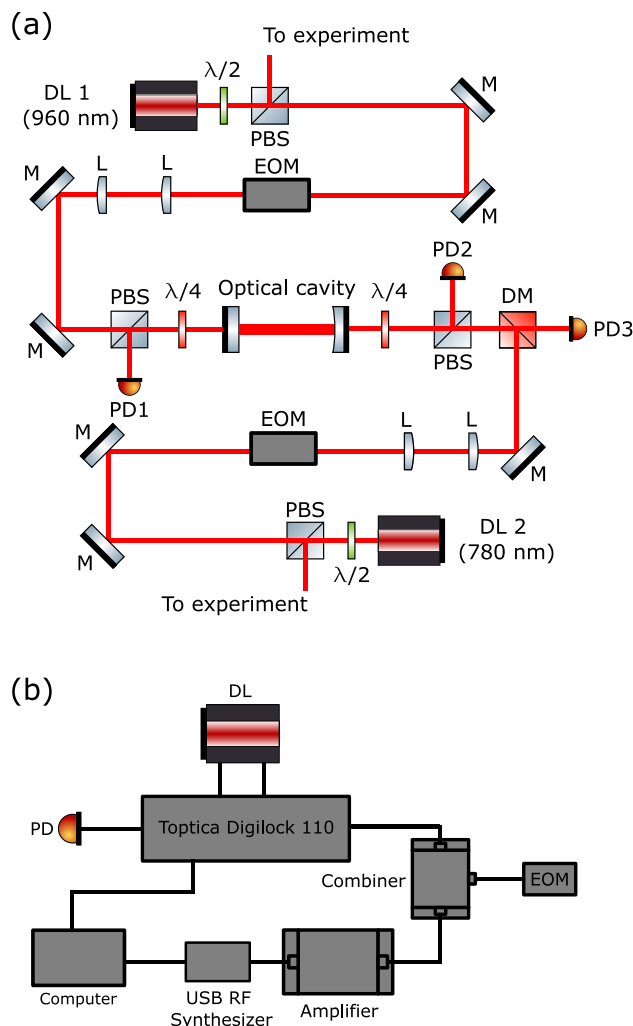


Fig. 4 Experimental setup for simultaneously locking the two cw tunable lasers (960 and 780 nm) in the same optical cavity, used the DSB locking technique. **a** Optical setup. **b** The electronic feedback circuit setup

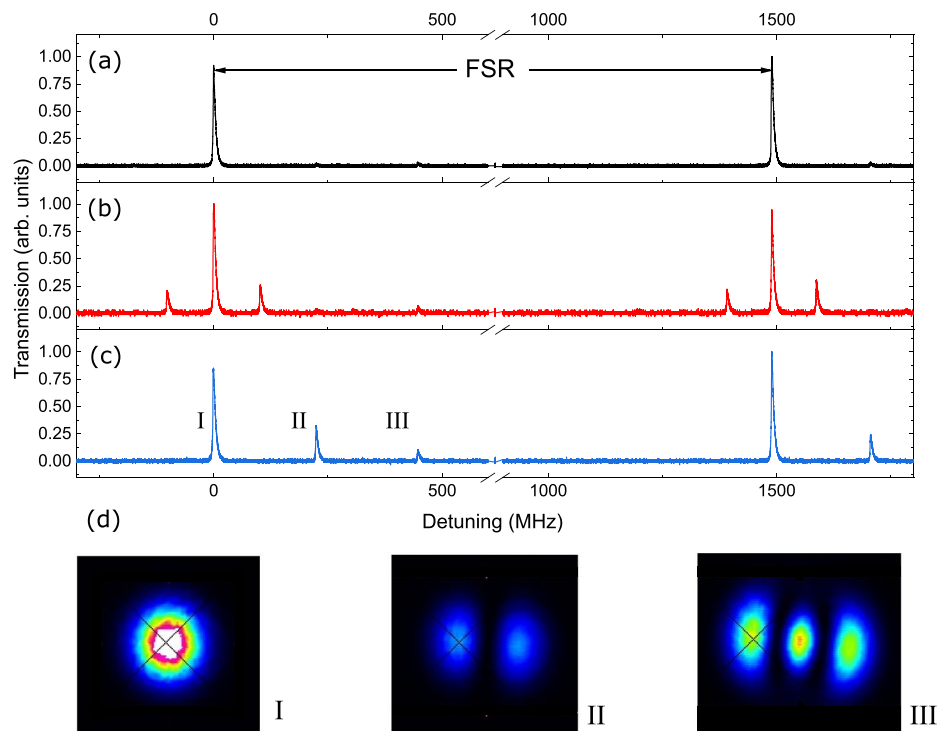
the best alignment to the fundamental mode of the cavity and to study the spectral properties of the cavity.

6 Cavity properties

6.1 Spectral characteristics

Initially, we have observed the transmission spectra using a digital oscilloscope, while the laser frequency was swept across two fundamental mode peaks. Figure 5a and b show the cavity spectra without and with moving sidebands at 100 MHz, respectively. In this case, a mode matching efficiency of 99% was obtained. Figure 5c shows the spectrum when the laser beam is slightly misaligned in the horizontal direction, exciting higher order modes. Figure 5d shows

Fig. 5 Transmission cavity spectra across two fundamental modes with a $\sim 99\%$ matching efficiency. **a** Without sidebands; **b** with moving sidebands at 100 MHz. **c** With a slightly misaligned laser beam, showing the HG₀₀ (peak I), HG₁₀ (peak II) and HG₂₀ (peak III). **d** Transverse beam profile for the HG₀₀, HG₁₀ and HG₂₀ modes (peaks I, II and III, respectively)



the transverse beam profile for the HG₀₀, HG₁₀ and HG₂₀ modes (peaks I, II and III, respectively). The frequencies of HG₁₀, HG₂₀ modes are shifted from the fundamental mode by approximately 15 and 30 % of the FSR, respectively [18].

The next step was to measure the cavity FSR using the fact that the right (I_R) and left (II_L) movable sidebands of adjacent fundamental modes (I_F and II_F), shown in Fig. 6a, overlaps when the modulation frequency is half of the FSR. Figure 6b shows the movable sidebands as a function of the laser PZT voltage for several EOM modulation frequencies. The laser PZT voltage difference (ΔV), between (I_R) and (II_L), is measured as a function of the modulation frequency, and shown in Fig. 6c. By a linear fitting, we obtain the intercept with the horizontal axis, and we obtained $\Delta v_{\text{FSR}} = 1497.6 \pm 0.1$ MHz, which is less than the expected $\Delta v_{\text{FSR}} = 1500$ MHz. To precisely calculate the FSR, it is necessary to take into account the curvature of one of the mirrors and its diameter, which increases the cavity length [11], leading to $\Delta v_{\text{FSR}} = 1496.6$ MHz.

Figure 7 shows the resonance in the transmission signal. Unfortunately, it does not allow us to obtain an accurate linewidth for the cavity because it is a convolution of the light transmission with the photodetector time response. One could imagine that the measurement of the radiation lifetime in the cavity would allow us to obtain the mirror reflection and, therefore, the finesse. However, for our case, the lifetime would be about 100 ns, and the photodetector time response would be an issue as well. So, we can only make a crude estimate of the linewidth of

Fig. 7, which is approximately 1 MHz (FWHM). By dividing Δv_{FSR} by the FWHM, we obtain ($\mathcal{F} \sim 1500$), which is enough to lock the lasers and reduce their linewidth to $\ll 1$ MHz.

6.2 Thermal stability and tuning

Typically, at room temperature, the thermal expansion coefficient (α) is well known for ULE and fused silica (FS), and are given by [19]:

$$\alpha_{\text{ULE}}(T) = \beta_{\text{ULE}}(T - T_0), \quad (2)$$

$$\alpha_{\text{FS}}(T) = 500 \times 10^{-9} \text{ K}^{-1} + \beta_{\text{FS}}(T - 294.15 \text{ K}), \quad (3)$$

where $\beta_{\text{ULE}} = 2.4 \times 10^{-9} \text{ K}^{-2}$ and $\beta_{\text{FS}} = 2.2 \times 10^{-9} \text{ K}^{-2}$ are the linear coefficients of thermal expansion of ULE and FS, respectively, and (T_0) is the zero-crossing temperature, around 21 °C for ULE. However, by combining a ULE spacer and fused silica mirrors, we obtain an effective thermal expansion coefficient (α_{eff}) for the cavity [20]. In the case of optically contacted mirrors, this effect is mainly due to the structural deformation of the mirror surfaces caused by the mismatch of the CTE of both materials. Following the approach described by Legero et al. [21], we can write the effective CTE of our cavity as

Fig. 6 Scheme for the FSR measurement by varying the moving sideband frequency of two adjacent modes. **a** Cavity reflection signal as a function of the laser PZT voltage around two fundamental modes (I_F and II_F) and their corresponding movable side bands (I_R and II_L). **b** Movable sidebands as a function of the laser PZT voltage for several EOM modulation frequencies. The laser PZT voltage difference (ΔV), between (I_R) and (II_L). **c** ΔV as a function of the modulation frequency. Experimental data is shown in black dots and the red line is a fitting

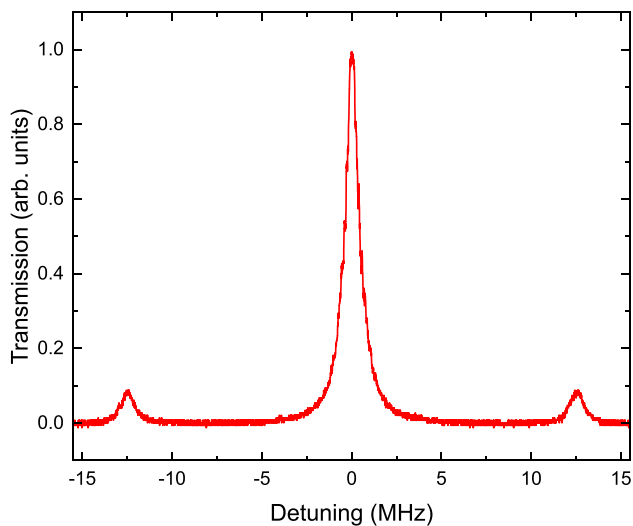
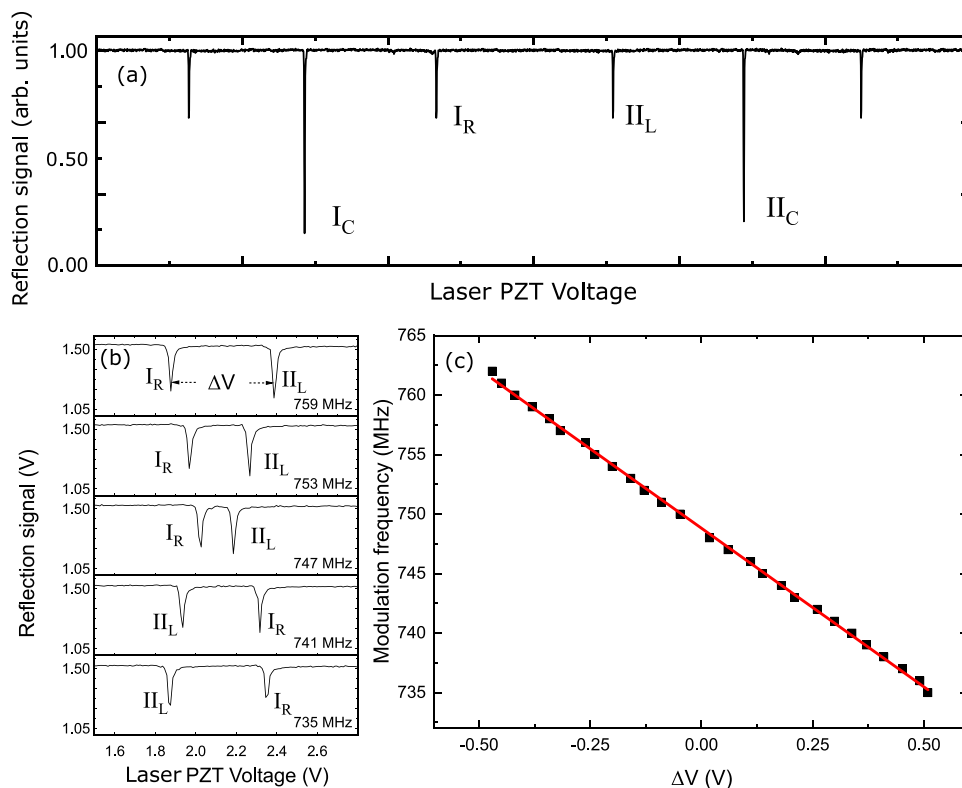


Fig. 7 Cavity transmission signal with sidebands at 12.5 MHz. The linewidth is estimated to be about 1 MHz

$$\alpha_{\text{eff}} = \alpha_{\text{ULE}} + 2\delta \frac{R}{L} (\alpha_{\text{FS}} - \alpha_{\text{ULE}}), \quad (4)$$

where δ is the coupling coefficient defined as the ratio between the longitudinal and radial expansion (dL/dR), and it depends only on the geometric and mechanical characteristics of the FS mirrors and the ULE spacer.

To quantify the thermal expansion of the cavity, we have set up an experiment. Figure 8 shows the cavity reflection signal (blue line) of a frequency scanning 780 nm laser and its saturated absorption spectroscopy (black line) over the $5S_{1/2} (F' = 2) \rightarrow 5P_{3/2}$ line of ^{87}Rb using a commercial equipment (model Cosy, TEM Messtechnik GmbH). The frequency difference ($\Delta\nu$) between the cavity peak and the crossover transition ($5S_{1/2} (F' = 2) \rightarrow 5P_{3/2} (F'' = 2 \text{ or } F'' = 3)$) was measured as a function of the temperature in the 15 – 30 °C range.

When the temperature setting is modified in the controller, the aluminum housing reaches thermal equilibrium in a few minutes. However, due to the poor thermal contact of the Viton rings, the cavity takes longer to reach thermal equilibrium. The inset of Fig. 9 shows $\Delta\nu$ as a function of time for a temperature change from 26 to 28 °C. The first decay time can be estimated as 30 min, while the second decay time is ≈ 3 h. To ensure that thermal equilibrium has been reached, we wait for the system to stabilize for 24 h after each temperature change, before taking a measurement. Figure 9 shows $\Delta\nu$ as a function of temperature, which presents a linear decrease with a slope of $m = 52.0 \pm 0.4$ MHz/K. Using this slope and Eq. (1), we can estimate an effective thermal expansion coefficient of $135 \times 10^{-9} \text{ K}^{-1}$. Also, we estimate $\delta \approx 1$. Our values for δ and α_{eff} are one order of magnitude higher compared to ultrastable cavities. This result is due to the combined effect of the geometry and dimensions of the cavity, the mirror substrate, and the glue used. The stability

Fig. 8 Cavity reflection signal (blue line) of a frequency scanning 780 nm laser and its saturated absorption spectroscopy (black line) over the $5S_{1/2} (F' = 2) \rightarrow 5P_{3/2}$ line of ^{87}Rb . ($\Delta\nu$) is the frequency difference between the cavity peak and the crossover transition

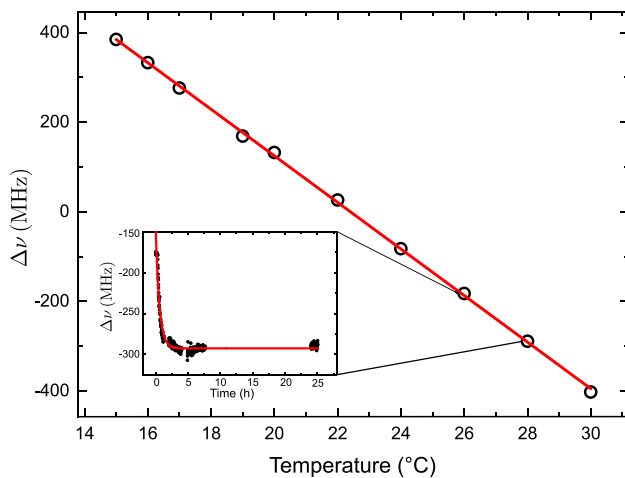
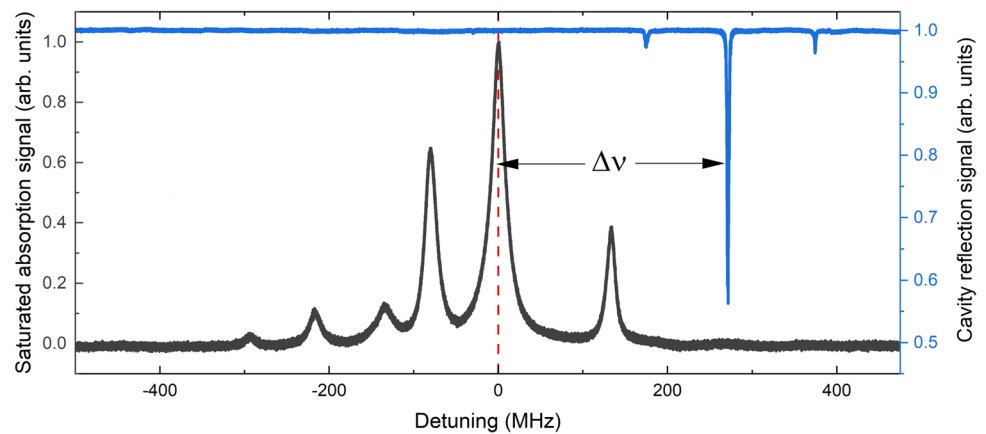


Fig. 9 $\Delta\nu$ as a function of the temperature in the 15–30 °C range. The inset shows $\Delta\nu$ as a function of time for a temperature change from 26 to 28 °C

of the temperature controller is about 4 mK, which represents a frequency stability of approximately 200 kHz for our cavity. This result suggests that a laser could be locked to any frequency to the cavity just by temperature tuning it without the use of an EOM.

7 Linewidth and long-term drift

Figure 10a shows the PDH signal, obtained from the Digilock module using a 25 MHz modulation. The central peak and valley are connected by a line (red line) with a slope of $D \sim 3.5 \text{ V/MHz}$. This signal is used to lock the laser, by optimizing the PID 1 and 2 feedback controllers from the Toptica module. Once the laser is locked, the error signal is monitored, as shown in Fig. 10b (blue dots), and it can be used to estimate the laser linewidth. We took a hundred thousand points, separated by 500 ns, which allowed us to

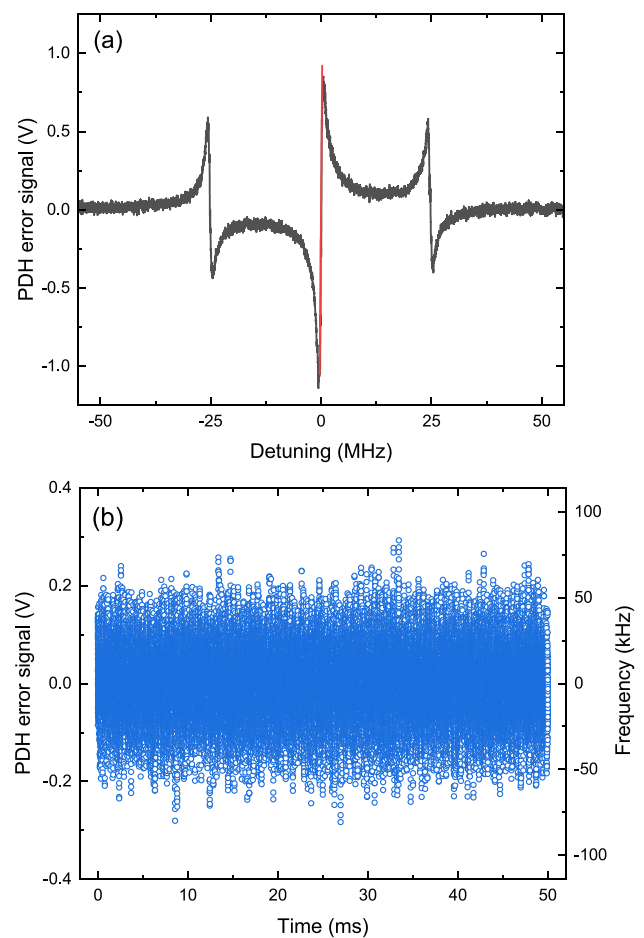


Fig. 10 **a** PDH error signal generated with a 25 MHz modulation. The red line is an estimation of the slope. **b** PDH error signal with the laser locked ($\Delta V_{\text{RMS}} \sim 0.07 \text{ V}$)

obtain a $\Delta V_{\text{RMS}} \sim 0.07 \text{ V}$. The RMS variation of the laser frequency is given by $\Delta\nu_{\text{RMS}} = \Delta V_{\text{RMS}}/D$. According to [22], the laser linewidth is $\Delta\nu_{\text{FWHM}} = 2.355\Delta\nu_{\text{RMS}}$, which is about $\approx 47 \text{ kHz}$ in our case. It is important to note that this procedure only allows us to obtain an upper limit for

the linewidth. A precise measurement requires a self heterodyning technique, however, this is outside the scope of this work. Nevertheless, it is important to note that [11] used a higher frequency bandwidth PDH electronics than us, therefore, it was expected that our linewidth would be larger.

Also, for our Rydberg experiments, an important parameter is the long-term stability of the laser source. However, the process of a “creep” in the crystallization of the different spacer material causes a slow and perpetual shortening of the cavity length [23]. In the case of ULE, the long-term drift (LTD) in resonant frequency has been estimated at approximately 10 kHz/day [6]. Other effects as the curing of the glue crept between the spacer and the mirrors of the cavity can produce an increase in the rate of the drift and also an expansion of the cavity length [11]. Depending on the experimental application and the long-term drift, this variation must be corrected daily by adjusting the movable sideband frequency. To measure the cavity long-term drift, we have monitored the resonant frequency of a fundamental mode, by locking the 780 nm laser frequency to a movable sideband. Then, the RF frequency of the movable sideband was tuned to maximize the saturation absorption transition $^{85}\text{Rb } 5S_{1/2} (F' = 3) \rightarrow 5P_{3/2} (F'' = 4)$ signal using a Cosy. This procedure allows us to measure the frequency difference between a fundamental mode and the atomic transition ($\Delta\nu_{\text{LTD}}$), during one month, under constant temperature conditions (18 °C). Figure 11 shows the experimental data (blue dots) of the frequency difference between ($\Delta\nu_{\text{LTD}}$) and the initial frequency ($\Delta\nu_{\text{LTD}}(t = 0)$) as a function of time. Using a linear fit (blue line in Fig. 11), we estimated a slope of

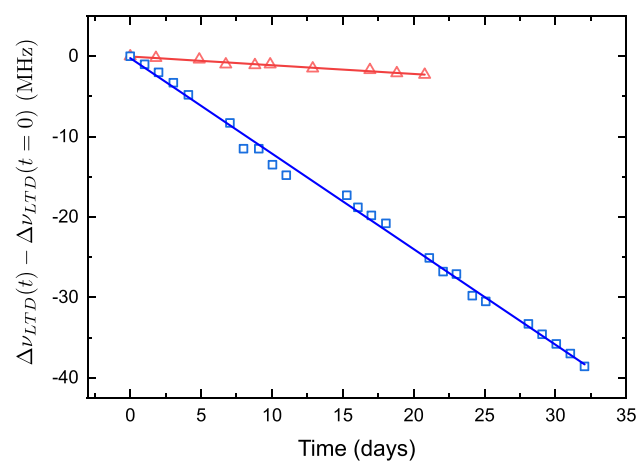


Fig. 11 Frequency difference ($\Delta\nu_{\text{LTD}}(t) - \Delta\nu_{\text{LTD}}(t = 0)$), between the relative frequency of a cavity fundamental mode with respect to the atomic frequency ($\Delta\nu_{\text{LTD}}(t)$) and its initial relative frequency ($\Delta\nu_{\text{LTD}}(t = 0)$), as a function of time. The blue points are the experimental data and the blue line is a linear fit for constant temperature conditions. The red dots are the experimental data and the red line is a linear fit when the temperature cavity is swept at a rate of 1.37 mK/h

1.19 ± 0.02 MHz/day. Since the frequency of the sideband decreases with time, the carrier frequency increases, so the cavity shrinks at a rate of 0.3 nm/day, which must be due to the curing of the epoxy glued mirror [11], since the other materials have a much smaller drift [6, 23]. To compensate for the natural cavity LTD, we have programmed the temperature controller to increase the temperature at a constant rate of 1.37 mK/h, and repeated the measurement. The data are shown by red dots in Fig. 11, presenting a long-term drift of 125 kHz/day. In principle, this temperature compensation technique could be improved, and eventually, the use of an EOM would no longer be required since the cavity could be temperature tuned.

8 EIT microwave spectrum

To demonstrate the usability of the constructed optical cavity and its robustness, we have set up a simple Electromagnetically Induced Transparency (EIT) experiment using a sample of atomic ^{85}Rb kept in a vapor cell at room temperature. Constant monitoring of a probe light gives us information on the transmission profile in response to microwave perturbations [12]. Figure 12a shows the atomic states and radiation fields involved. The probe laser, operating at 780 nm, is frequency locked to the optical cavity in the $5S_{1/2} (F' = 3) \rightarrow 5P_{3/2} (F'' = 4)$ transition, its detuning (Δ_p) is set 0 MHz and Rabi frequency (Ω_p) to 2.2 MHz. A control laser, at 480 nm, connects an intermediate state $5P_{3/2} (F'' = 4) \rightarrow 68S_{1/2}$, its detuning (Δ_c) is set 0 Hz and Rabi frequency (Ω_p) to 3.5 MHz. This light is generated by second-harmonic generation (SHG) of a 960 nm diode laser. The 960 nm laser is also frequency locked to the same cavity (dual locking). A microwave photon is used to observe the opening windows of EIT and EIA (Electromagnetic Induced Absorption) throughout the probe beam [24]. A microwave generator feeds a microwave horn to drive the $68S_{1/2} \rightarrow 68P_{3/2}$ transition (Fig. 12b). To increase the signal-to-noise ratio, the microwave generator is modulated at 1 kHz, and the transmitted signal from the probe is processed by a lock-in amplifier [25]. Figure 13 shows the normalized probe transmission signal as a function of microwave frequency and normalized microwave power. The plot illustrates a complex relationship between microwave power and frequency, leading to an increase in transparency (EIT) and absorption (EIA). Such spectra are typical of multiphotonic quantum interference [26]. In particular, it is possible to observe two microwave photon transition around 11.779 MHz ($68S_{1/2} \rightarrow 69S_{1/2}$).

To estimate the linewidth of the 480 nm laser, we have investigated this transition in more detail as a function of microwave power. Figure 14a shows the EIT spectrum as a function of the microwave frequency for the highest and

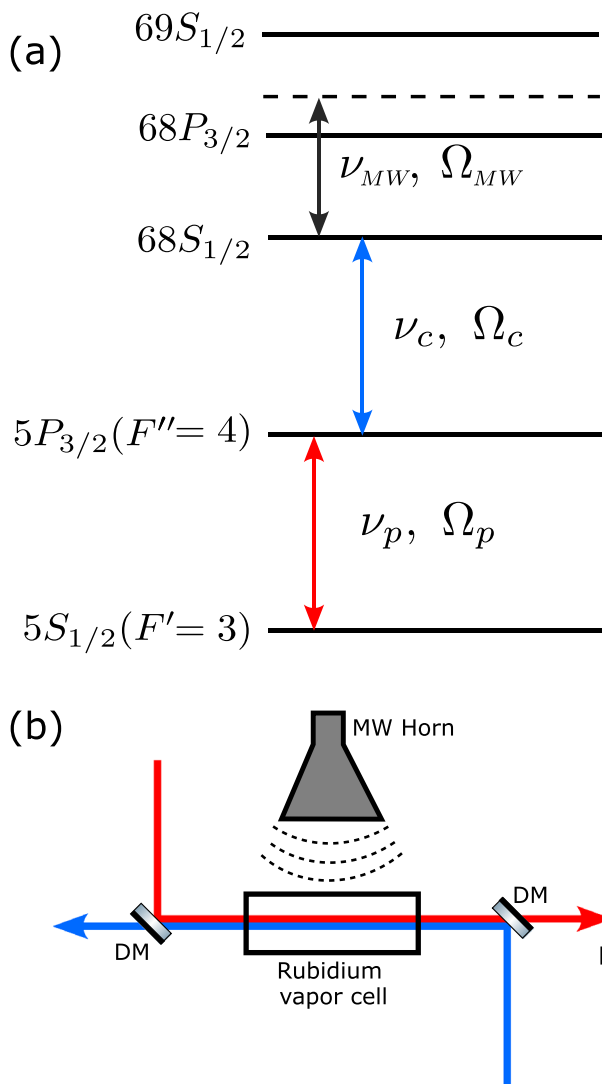


Fig. 12 **a** Scheme of the five-level atom and the radiation fields involved in the experiment. States $5S_{1/2}$ ($F' = 3$) and $5P_{3/2}$ ($F'' = 4$) are coupled by the probe laser, states $5P_{3/2}$ ($F'' = 4$) and $68S_{1/2}$ are coupled by the control laser. States $68S_{1/2}$, $68P_{3/2}$ and $69S_{1/2}$ are Rydberg levels, connected by microwave radiation. **b** Experimental setup (not to scale): Dichroic mirrors (DM), microwave horn, vapor cell, and photodetector (PD). A probe and control lasers counterpropagate inside a rubidium vapor cell under the influence of an MW field generated at the MW horn

lowest microwave power. Clearly, the transition linewidth ($\Delta\nu_{\text{TP}}$) is broadened by the microwave power. Figure 14b shows $\Delta\nu_{\text{TP}}$ as a function of normalized microwave power, which presents a linear dependence, which presents a linear dependence. By extrapolating the fit, we obtain $\Delta\nu_{\text{TP}} = 133 \pm 15$ kHz for zero microwave power. The linewidth is limited by the 480 nm laser linewidth, the Rydberg $S_{1/2}$ state linewidths involved in the transition, Doppler effect, etc. For our case, the estimated 480 nm laser linewidth is about 100 kHz, and the states involved have

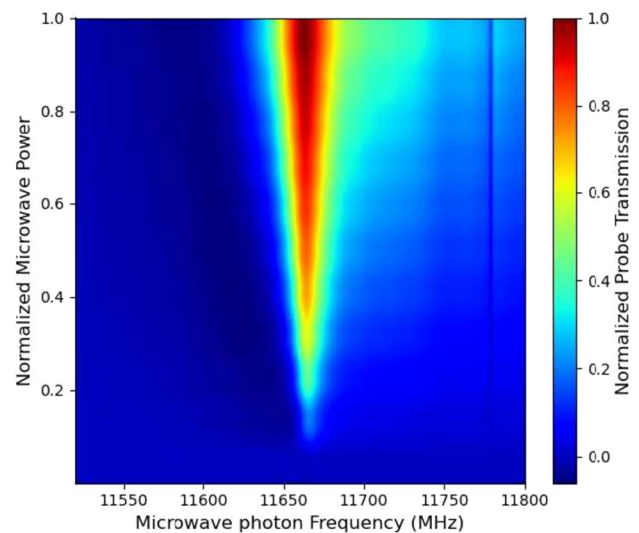


Fig. 13 $68S_{1/2}$ state EIT probe transmission signal as a function of the microwave frequency and its power

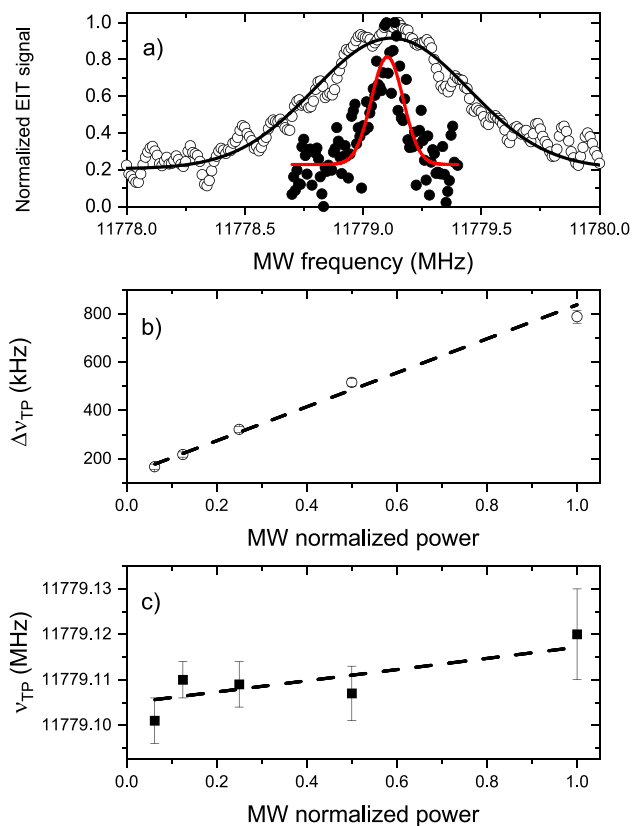


Fig. 14 **a** EIT spectrum as a function of the microwave frequency for the highest (open circles) and lowest (black circles) microwave power. The lines are Gaussian fittings. **b** The transition linewidth ($\Delta\nu_{\text{TP}}$) and **c** central frequency (ν_{TP}) of the two photon transition a function of normalized microwave power

linewidths of about 10 kHz. Therefore, the obtained $\Delta\nu_{\text{TP}}$ is consistent with our experimental setup. Figure 14c shows the center frequency (ν_{TP}) of the two photon transition as a function of normalized microwave power. By extrapolating the fitting, we obtain $\nu_{\text{TP}} = 11779.105 \pm 0.004$ MHz, which is in very good agreement with the calculated value ($\nu_{\text{TP}} = 11779.11$ MHz) [27].

9 Conclusions

In this work, we have constructed and characterized an affordable medium-finesse optical cavity ($\mathcal{F} \sim 1500$), to simultaneously stabilize two cw tunable diode lasers at 780 and 960 nm. We have provided a simple recipe for its construction and characterization. Its temperature is controlled using TEC elements inside a high-vacuum chamber, which allows us to tune a full FSR of the cavity in the 15–30 °C range. We were able to lock the lasers at any frequency within the cavity free spectral range (FSR) using the Pound–Drever–Hall technique (PDH). We have measured the long-term drift of the cavity, which is about 1.2 MHz/day. We have also demonstrated that it can be compensated for by methodically controlling temperature variation. Finally, we have demonstrated its use in an EIT experiment using a two photon Rydberg microwave spectroscopy, the system allowed us to observe linewidths down to 130 kHz. Certainly, the current configuration is versatile and suitable for both atom cooling and trapping, as well as Rydberg atom physics experiments. We should point that our present system linewidth is limited by the locking electronics only, but that is not an issue for Rydberg physics in thermal samples [13].

Acknowledgements This work is supported by grants 2018/06835-0, 2019/23510-0, 2019/10971-0, 2021/04107-0, 2021/06371-7 and 2022/16904-5, São Paulo Research Foundation (FAPESP) and CNPq (305257/2022-6). It is also supported by the US Air Force Office of Scientific Research (Grant FA9550-20-1-0031) and the Army Research Office (Grant W911NF-21-1-0211).

Data availability The experimental data are available from the authors upon reasonable request.

References

- C.L. Mueller, M.A. Arain, G. Ciani, R.T. DeRosa, A. Effler, D. Feldbaum, V.V. Frolov, P. Fulda, J. Gleason, M. Heintze, K. Kawabe, E.J. King, K. Kokeyama, W.Z. Korth, R.M. Martin, A. Mullavey, J. Peold, V. Quetschke, D.H. Reitze, D.B. Tanner, C. Vorvick, L.F. Williams, G. Mueller, The advanced LIGO input optics. *Rev. Sci. Instrum.* **87**(1), 014502 (2016). <https://doi.org/10.1063/1.4936974>
- T. Bothwell, C.J. Kennedy, A. Aeppli, D. Kedar, J.M. Robinson, E. Oelker, A. Staron, J. Ye, Resolving the gravitational redshift across a millimetre-scale atomic sample. *Nature* **602**, 420–424 (2022). <https://doi.org/10.1038/s41586-021-04349-7>
- X. Zheng, J. Dolde, V. Lochab, B.N. Merriman, H. Li, S. Kolkowitz, Differential clock comparisons with a multiplexed optical lattice clock. *Nature* **602**, 425–430 (2022). <https://doi.org/10.1038/s41586-021-04344-y>
- M.W. Hamilton, An introduction to stabilized lasers. *Contemp. Phys.* **30**, 21–33 (1989). <https://doi.org/10.1080/00107518908222588>
- A. Javan, W.R. Bennett, D.R. Herriott, Population inversion and continuous optical maser oscillation in a gas discharge containing a he-ne mixture. *Phys. Rev. Lett.* **6**, 106–110 (1961). <https://doi.org/10.1103/PhysRevLett.6.106>
- J.L. Hall, Frequency-stabilized Lasers: A Parochial Review. *Frequency-Stabilized Lasers and Their Applications*, vol. 1837 (SPIE, 1993), p. 2. <https://doi.org/10.1117/12.143668>
- P.H. Lee, M.L. Skolnick, Saturated neon absorption inside a 6238-Å laser. *ApPhL* **10**, 303–305 (1967). <https://doi.org/10.1063/1.1754821>
- C. Wieman, T.W. Hänsch, Doppler-free laser polarization spectroscopy. *Phys. Rev. Lett.* **36**, 1170 (1976). <https://doi.org/10.1103/PhysRevLett.36.1170>
- M.L. Eickhoff, J.L. Hall, Optical frequency standard at 532 nm. *IEEE Trans. Instrum. Meas.* **44**, 155–158 (1995). <https://doi.org/10.1109/19.377797>
- R.W.P. Drever, J.L. Hall, F.V. Kowalski, J. Hough, G.M. Ford, A.J. Munley, H. Ward, Laser phase and frequency stabilization using an optical resonator. *Appl. Phys. B* **31**, 97–105 (1983). <https://doi.org/10.1007/BF00702605/METRICS>
- J. Hond, N. Cisternas, G. Lochead, N.J. Druten, Medium-finesse optical cavity for the stabilization of rydberg lasers. *Appl. Opt.* **56**, 5436 (2017). <https://doi.org/10.1364/AO.56.005436>
- J.A. Sedlacek, A. Schwettmann, H. Kübler, R. Löw, T. Pfau, J.P. Shaffer, Microwave electrometry with rydberg atoms in a vapour cell using bright atomic resonances. *Nat. Phys.* **8**(11), 819–824 (2012). <https://doi.org/10.1038/nphys2423>
- R. Finkelstein, S. Bali, O. Firstenberg, I. Novikova, A practical guide to electromagnetically induced transparency in atomic vapor. *New J. Phys.* **25**(3), 035001 (2023). <https://doi.org/10.1088/1367-2630/acbc40>
- Ule ® corning code 7972 ultra low expansion glass advanced optics and materials ule ® corning code 7972 ultra low (2006). <http://www.corning.com/media/worldwide/csm/documents/D20FD2EA-7264-43DD-B544-E1CA042B486A.pdf>
- C.E. Powers, *Outgassing Data for Selected Spacecraft Materials* (NASA, 2014). <http://outgassing.nasa.gov/>
- J.I. Thorpe, K. Numata, J. Livas, Laser frequency stabilization and control through offset sideband locking to optical cavities. *Opt. Express* **16**(20), 15980–15990 (2008). <https://doi.org/10.1364/OE.16.015980>
- E.D. Black, An introduction to Pound-Drever–Hall laser frequency stabilization. *Am. J. Phys.* **69**(1), 79–87 (2001). <https://doi.org/10.1119/1.1286663>
- H. Kogelnik, T. Li, Laser beams and resonators. *Appl. Opt.* **5**, 1550 (1966). <https://doi.org/10.1364/ao.5.001550>
- M.D. Álvarez, Optical cavities for optical atomic clocks, atom interferometry and gravitational-wave detection. Springer, Cham, pp. 1–245. <https://doi.org/10.1007/978-3-030-20863-9>
- J. Zhang, Y.X. Luo, B. Ouyang, K. Deng, Z.H. Lu, J. Luo, Design of an optical reference cavity with low thermal noise and flexible thermal expansion properties. *Eur. Phys. J. D* **67**, 825 (2012). <https://doi.org/10.1140/epjd/e2013-30458-2>

21. T. Legero, U. Sterr, T. Kessler, Tuning the thermal expansion properties of optical reference cavities with fused silica mirrors. *JOSA B* **27**(5), 914–919 (2010). <https://doi.org/10.1364/JOSAB.27.000914>
22. C. Qiao, C.Z. Tan, F.C. Hu, L. Couturier, I. Nosske, P. Chen, Y.H. Jiang, B. Zhu, M. Weidemüller, An ultrastable laser system at 689 nm for cooling and trapping of strontium. *Appl. Phys. B Lasers Opt.* **125**, 215 (2019). <https://doi.org/10.1007/s00340-019-7328-3>
23. I. Ito, A. Silva, T. Nakamura, Y. Kobayashi, Stable CW laser based on low thermal expansion ceramic cavity with 49 mhz/s frequency drift. *Opt. Express* **25**, 26020 (2017). <https://doi.org/10.1364/oe.25.026020>
24. J.M. Kondo, N. Šibalić, A. Guttridge, C.G. Wade, N.R.D. Melo, C.S. Adams, K.J. Weatherill, Observation of interference effects via four-photon excitation of highly excited rydberg states in thermal cesium vapor. *Opt. Lett.* **40**(23), 5570–5573 (2015). <https://doi.org/10.1364/OL.40.005570>
25. X. Liu, F. Jia, H. Zhang, J. Mei, Y. Yu, W. Liang, J. Zhang, F. Xie, Z. Zhong, Using amplitude modulation of the microwave field to improve the sensitivity of rydberg-atom based microwave electrometry. *AIP Adv.* **11**(8), 085127 (2021). <https://doi.org/10.1063/5.0054027/967158>
26. D. McGloin, D.J. Fulton, M.H. Dunn, Electromagnetically induced transparency in n-level cascade schemes. *Opt. Commun.* **190**(1), 221–229 (2001). [https://doi.org/10.1016/S0030-4018\(01\)01053-7](https://doi.org/10.1016/S0030-4018(01)01053-7)
27. E.J. Robertson, N. Šibalić, R.M. Potvliege, M.P.A. Jones, Arc 3.0: an expanded python toolbox for atomic physics calculations. *Comput. Phys. Commun.* **261**, 107814 (2021). <https://doi.org/10.1016/j.cpc.2020.107814>

Publisher's Note Springer Nature remains neutral with regard to jurisdictional claims in published maps and institutional affiliations.

Springer Nature or its licensor (e.g. a society or other partner) holds exclusive rights to this article under a publishing agreement with the author(s) or other rightsholder(s); author self-archiving of the accepted manuscript version of this article is solely governed by the terms of such publishing agreement and applicable law.